



An electron paramagnetic resonance study of the ethylammonium-, methylammonium-, and acetamidinium-tetrachlorocuprates
by Paul Henry Amundson

A thesis submitted to the Graduate Faculty in partial fulfillment of the requirements for the degree of
MASTER OF SCIENCE in Physics
Montana State University
© Copyright by Paul Henry Amundson (1968)

Abstract:

A K-band electron paramagnetic resonance spectrometer was constructed in order to determine the high and low field g -values, line shapes, and line widths for the spectra of divalent copper in ethylammonium-tetrachlorocuprate and methylammonium-tetrachlorocuprate. The g -tensors were determined to be $g_{xx} = 2.053$, $g_{yy} = 2.067$, and $g_{zz} = 2.261$ for ethylammonium-tetrachlorocuprate and $g_{xx} = 2.054$, $g_{yy} = 2.067$, and $g_{zz} = 2.271$ for methylammonium-tetrachlorocuprate. An exchange frequency of 20.39 GHz for ethylammonium-tetrachlorocuprate and 17.48 GHz for methylammonium-tetrachlorocuprate was computed. Data was also taken on acetamidinium-tetrachlorocuprate to confirm earlier findings.

154

AN ELECTRON. PARAMAGNETIC RESONANCE STUDY OF THE ETHYLAMMONIUM-,
METHYLAMMONIUM-, AND ACETAMIDINIUM-TETRACHLOROCUPRATES

by

PAUL HENRY AMUNDSON

A thesis submitted to the Graduate Faculty in partial
fulfillment of the requirements for the degree

of

MASTER OF SCIENCE

in

Physics

Approved:

N. L. Moise

Head, Major Department

John E. Cunningham

Chairman, Examining Committee

J. K. Goering

Graduate Dean

MONTANA STATE UNIVERSITY
Bozeman, Montana

December, 1968

Acknowledgements

The author gratefully acknowledges the financial support of Montana State University (1966-67), of the Naval Weapons Center (1967-68), and of the National Science Foundation (Summer, 1968).

He is extremely grateful to Professor John E. Drumheller, whose advice and encouragement were instrumental in the accomplishment of the work. The author also wishes to thank F. J. Blankenburg for the design and construction of the modulation oscillation amplifier and Professor K. Emerson for growing the crystals studied.

Table of Contents

Chapter	Page
Abstract	vii
I. Introduction	1
II. EPR of Copper Complexes	5
III. Experimental Results	9
IV. The Spectrometer	
The Spectrometer	17
Operation of the Spectrometer	26
V. Appendix	31
Literature Cited	34

List of Tables

Table	Page
I. Experimental Results	9
II. G-values	15
II. Gaussian and Lorentzian Theoretical Data Points	33

List of Figures

Figure		Page
1.	Energy Level Diagram for Divalent Copper	4
2.	Distorted Octahedral Symmetry	7
3.a,b	Crystal Structures of EATCC, MATCC, and ACTCC	8
4.	EATCC Experimental and Theoretical Curves (low field)	10
5.	EATCC Experimental and Theoretical Curves (high field)	11
6.	MATCC Experimental and Theoretical Curves (low field)	12
7.	MATCC Experimental and Theoretical Curves (high field)	13
8.	ACTCC Representative Experimental Curve	14
9.	Block Diagram of the Spectrometer	18
10.	Circuit Diagram for 125 KHz Amplifier	20
11.	Circuit Diagram for 125 KHz Oscillator-Amplifier	21
12.	Variable Temperature Cavity Mount	23
13.	24.7 GHz Microwave Cavity	24
14.	Klystron Mode with Cavity Resonance	27
15.	NMR Resonance Signal	300

Abstract

A K-band electron paramagnetic resonance spectrometer was constructed in order to determine the high and low field g-values, line shapes, and line widths for the spectra of divalent copper in ethylammonium-tetrachlorocuprate and methylammonium-tetrachlorocuprate. The g-tensors were determined to be $g_{xx} = 2.053$, $g_{yy} = 2.067$, and $g_{zz} = 2.261$ for ethylammonium-tetrachlorocuprate and $g_{xx} = 2.054$, $g_{yy} = 2.067$, and $g_{zz} = 2.271$ for methylammonium-tetrachlorocuprate. An exchange frequency of 20.39 GHz for ethylammonium-tetrachlorocuprate and 17.48 GHz for methylammonium-tetrachlorocuprate was computed. Data was also taken on acetamidinium-tetrachlorocuprate to confirm earlier findings.

Chapter I: Introduction

Electron paramagnetic resonance (EPR) has been a useful tool of the spectroscopist since the first experiments of Zavoisky in 1944.¹ The improvements in microwave equipment have given continuing impetus to the application of EPR to the solution of problems in a wide range of disciplines, including biology, chemistry, engineering and physics.

Classically, the spinning electron in a magnetic field has been compared to a spinning top precessing in the gravitational field of the earth.² A simple quantum mechanical treatment will be given here. Consider the magnetic moment, $\vec{\mu} = g\beta\vec{s}$, associated with the spin, \vec{s} , of an electron, where g is the spectroscopic splitting factor or Lande g -factor (2.0023 for free electrons) and β is the Bohr magneton ($\beta = 0.92731 \times 10^{-20}$ erg/gauss).^{3,4} Quantum mechanically, μ can assume $2S + 1$ discrete orientations in a static homogeneous magnetic field, \vec{H}_0 , according to the Zeeman interaction $H_z = g\beta\vec{H}_0 \cdot \vec{s}$. Each of the orientations corresponds to an energy level in the system. A small perturbing magnetic field, \vec{H}_1 , perpendicular to \vec{H}_0 and "rotating" about \vec{H}_0 with a frequency ν , provides the energy for transitions among these levels. The condition for resonant absorption is given by the following equation: $h\nu = g\beta H_0$, where h is Planck's constant ($6.625 \cdot 7 \times 10^{-27}$ erg-s). The z axis is generally chosen to be along the field \vec{H}_0 , while \vec{H}_1 is a small linearly oscillating field which appears to rotate in the plane perpendicular to \vec{H}_0 . \vec{H}_1 can be resolved into two counter-rotating fields in the same plane. The component which rotates opposite to the Larmor precessional direction has little effect; however, the other component can be absorbed and can cause transitions. The terms for the Hamiltonian can then be written as follows: $H_z =$

$g\beta S_z H_0$ and $H_{\text{pert.}} = g\beta S_x H_1 \cos 2\pi\nu t$ where S_z and S_x are the z and x axis projections of the spin. S_x can be rewritten as $S_+ + S_-$ if S_+ and S_- are defined as follows: $S_+ = \frac{S_x + iS_y}{2}$ and $S_- = \frac{S_x - iS_y}{2}$. Let $|M\rangle$ represent a state of the system, where M is the electron spin magnetic number, and operate on this set with $H_{\text{pert.}}$. It is then seen that transitions to higher and lower spin states are possible. $H_{\text{pert.}} |M\rangle = g\beta H_1 \cos 2\pi\nu t (S_+ + S_-) |M\rangle = g\beta H_1 \cos 2\pi\nu t \left[\frac{\hbar}{2} (\sqrt{S(S+1) - M(M+1)} |M+1\rangle + \sqrt{S(S+1) - M(M-1)} |M-1\rangle) \right]$. The line intensity of transition probability per unit time for the state $|M-1\rangle$ is proportional to the matrix element squared. Intensity $\sim | \langle M-1 | H_{\text{pert.}} | M \rangle |^2 = \frac{\hbar^2 g^2 \beta^2}{4} |\cos 2\pi\nu t|^2 [S(S+1) - M(M-1)]$. Briefly, \vec{H}_0 splits the spin degenerate levels and \vec{H}_1 provides the energy for transitions. Transitions take place only if the rotational frequency of \vec{H}_1 about the z axis is the same as the rotational frequency (Larmour frequency) of the magnetic moment.

In addition to the magnetic moment of the electron, many atoms have a nuclear magnetic moment which can be defined as $\vec{\mu}_N = g_N \beta_N \vec{I}$, where \vec{I} is the nuclear spin. The effect of this term can be considered as an interaction perturbation in the Hamiltonian and can be written as $A \vec{S} \cdot \vec{I}$, where A is a constant. The nucleus of the copper atom has a spin of 3/2 which should give a hyperfine spectrum; however, experimentally this is concealed by the spin-spin broadening of the hyperfine transition.⁵

The electron in a crystal lattice is not free as was the case in the preceding discussion; it is constrained by various interaction and binding forces. The paramagnetic ion considered in this thesis was divalent copper (Cu^{++}). Cu^{++} is in the iron transition group and has an electronic con-

figuration $1s^2 2s^2 2p^6 3s^2 3p^6 3d^9$.³ In solids the electronic orbital motion interacts with the crystalline electric fields and becomes decoupled from the spin.³ This is called quenching and is a strong mechanism in the iron group. As a result, in Cu^{II} the ground state ion is only spin degenerate. The ground state is the $x^2 - y^2$ orbital. Figure One shows a schematic diagram of the energy levels of divalent copper.⁶ This figure shows that the free ion level is orbitally five-fold degenerate and two-fold spin degenerate. When the ion is placed in a cubically symmetric electric field, it splits into two energy levels, the top one of which is three-fold orbitally degenerate. The addition of a tetragonal component to the electric field further reduces the orbital degeneracy. Finally, spin orbit coupling eliminates the orbital degeneracy. Application of a magnetic field removes the spin degeneracy of all levels but is shown here only for the lowest level.

The Jahn-Teller theorem states that a crystal lattice will distort to remove as much degeneracy as possible.^{3,7} Kramer's theorem states that if there are an odd number of electrons in the system, no electric field can remove all the degeneracy of the states.⁸ The ground state of Cu^{II} before application of the magnetic field is doubly degenerate and is split 852 cm^{-1} from the nearest excited orbital state.³ At room temperature only a few electrons have enough energy to jump an energy gap of more than 250 cm^{-1} so that there are very few electrons occupying the excited orbital levels. Therefore, the only extensively populated levels are the spin degenerate ground orbital singlet state.

Numbers on each energy level indicate orbital and spin degeneracy respectively of each level.

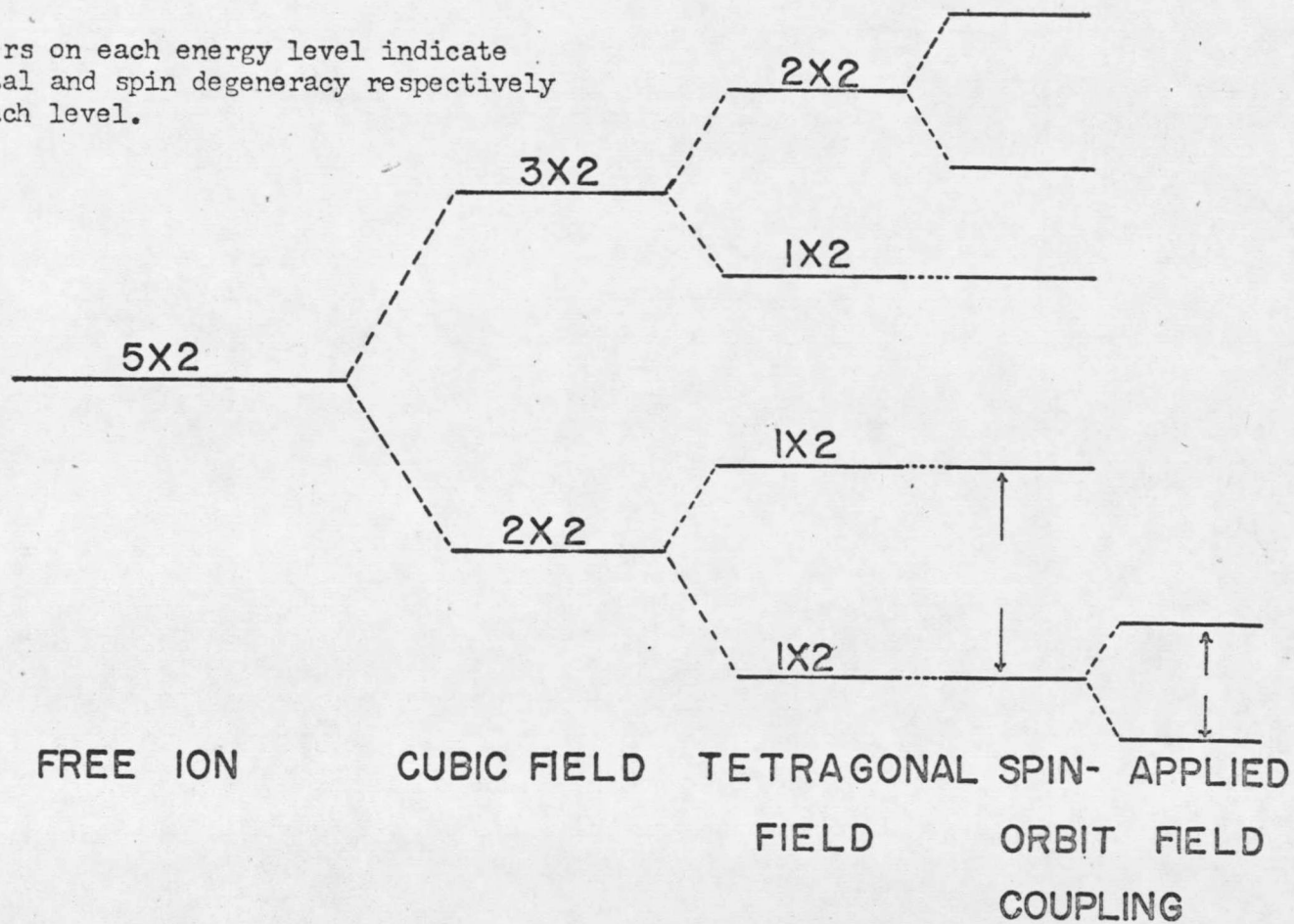


Figure 1. Energy level diagram for divalent copper

Chapter II: EPR of Copper Complexes.

Cu^{++} is one of the ideal ions for paramagnetic resonance since there is only one electronic transition and narrow lines can be obtained at room temperatures.

Historically, most new discoveries associated with solid state microwave spectra have been first observed in Cu^{++} salts. "The effect of exchange forces was first discovered in $\text{CuSO}_4 \cdot 5\text{H}_2\text{O}$; the existence of hyperfine structure was first observed in a diluted copper salt; the effect of the quadrupole interaction was first noticed in the Cu^{++} hyperfine spectrum; heavy water was first used with copper Tutton salt crystals to resolve out the isotope splitting; the concept of a resonating crystal field was first introduced to account for the copper fluosilicate spectrum; and measurements on copper acetate were the first to show that two paramagnetic ions could interact strongly to form a combined system of energy levels."⁵

Ethylammonium-tetrachlorocuprate [EATCC , $(\text{C}_2\text{H}_5\text{NH}_3)_2\text{CuCl}_4$] and methylammonium-tetrachlorocuprate [MATCC , $(\text{CH}_3\text{NH}_3)_2\text{CuCl}_4$] have been studied to obtain preliminary information regarding the g values, line shapes, and line widths at room temperatures.⁹ The present work has shown previously found g values to be incorrect because the g values tended towards Willett's for misalignment of the crystal.¹⁰ In addition, the line widths and line shapes which were determined in this work did not appear in the previous results.

The unusual "two dimensional" crystal structure found in EATCC and MATCC has stimulated interest in these and other similar crystals.

Figure Two shows an exaggerated and distorted octahedral symmetry particular to EATCC and MATCC. The axes x, y, and z are associated with the shortest to longest bonds respectively. In MATCC and EATCC, the bond lengths are $x = 2.300 \text{ \AA}$, $y = 2.332 \text{ \AA}$ and $z = 2.793 \text{ \AA}$.¹¹ In acetamidinium-tetrachlorocuprate (ACTCC, $[\text{CH}_3\text{C}(\text{NH}_2)_2 \text{CuCl}_4]$), the x and y bond lengths are approximately equal and the z bond length is longer.

Figure Three, a. and b. points out the structure in EATCC, MATCC, and ACTCC. The broad face of the crystals is parallel to the plane of the paper in Figure Three. The z axis in a. is the long bond and in b. the z axis is perpendicular to the plane shown. The Cu^{++} ions are represented as dots in both a. and b. The chlorine ions can be thought of as appearing at the end of each linear bond representation in a. and in the middle of each linear representation in b.

The data from the work on EATCC and MATCC has been used for a preliminary study of the exchange mechanism between the Cu^{++} ions with Cl^- as a bridge. This exchange mechanism is generally referred to as "super exchange."¹³ This data will later be used as part of a frequency dependent study of g values. ACTCC was studied to confirm the existence of a second magnetic axis in the crystal.^{9,12,13} The g values of ACTCC have been measured and are included with the results.¹² A representative ACTCC line shape is also included.

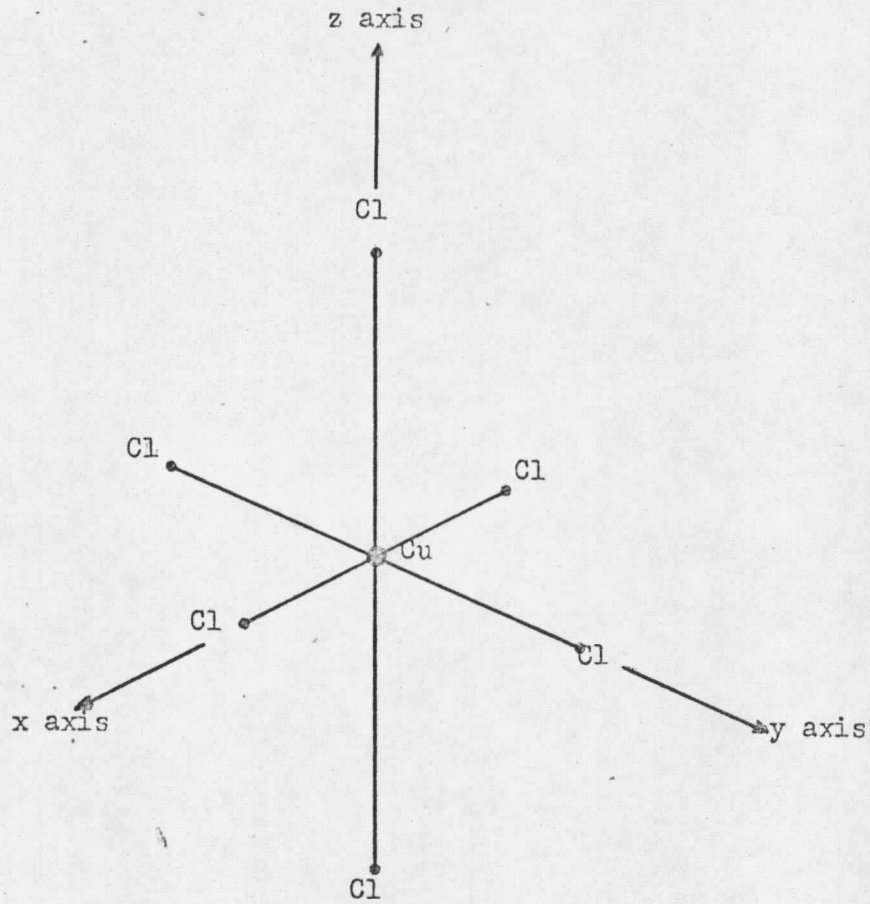
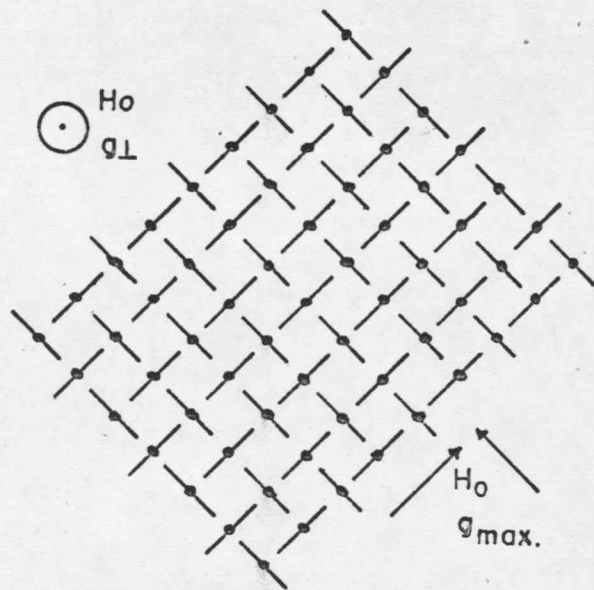
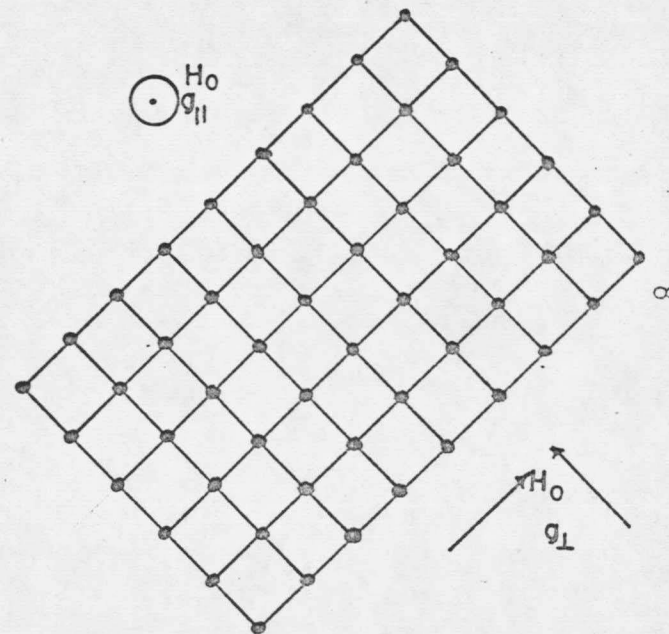


Figure 2. Distorted Octahedral Symmetry Particular to EATCC and MATCC



yz plane
 —●— long bond
 Cu

Figure 3-a. Crystal Structure of EATCC, MATCC



xy plane
 —●— short bonds
 Cu

Figure 3-b. Crystal Structure of ACTCC

Chapter III: Experimental Results

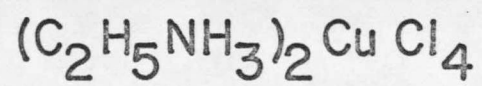
EATCC, MATCC, and ACTCC were studied with the k-band spectrometer.

The maximum and minimum g values, line widths, and line shapes were taken for EATCC and MATCC. In addition, the existence of a second magnetic axis in ACTCC was confirmed with this spectrometer. This data is presented in Table I and in Figures Four through Eight. The theoretical Lorentzian and Gaussian line shapes are superimposed on the experimental line shapes of EATCC and MATCC. (It should be noted that in opposition to the usual custom, the theoretical shapes are represented as circles and crosses while the experimental data are continuous. This is because the experimental data are traced from the chart recorder output of the spectrometer.)

TABLE I

Crystal	g min	g max	line width g min gauss	line width g max gauss
EATCC	2.053	2.164	80.2	84.1
EATCC ^W	2.044	2.137		
MATCC	2.054	2.169	94.9	99.4
MATCC ^W	2.046 2.047	2.143 2.141		
ACTCC ¹	2.337 exch. 2.355 isol.	2.061 2.063		

W-The data of Willett et al. on EATCC, MATCC is included for comparison.¹⁰



LOW FIELD (g max.)

EXP. CURVE ———

THEOR. GAUSSIAN ○ ○ ○ ○

THEOR. LORENTZIAN × × × ×

7850

8000

8150

8300

8450

8600

GAUSS

10

Figure 4. EATCC

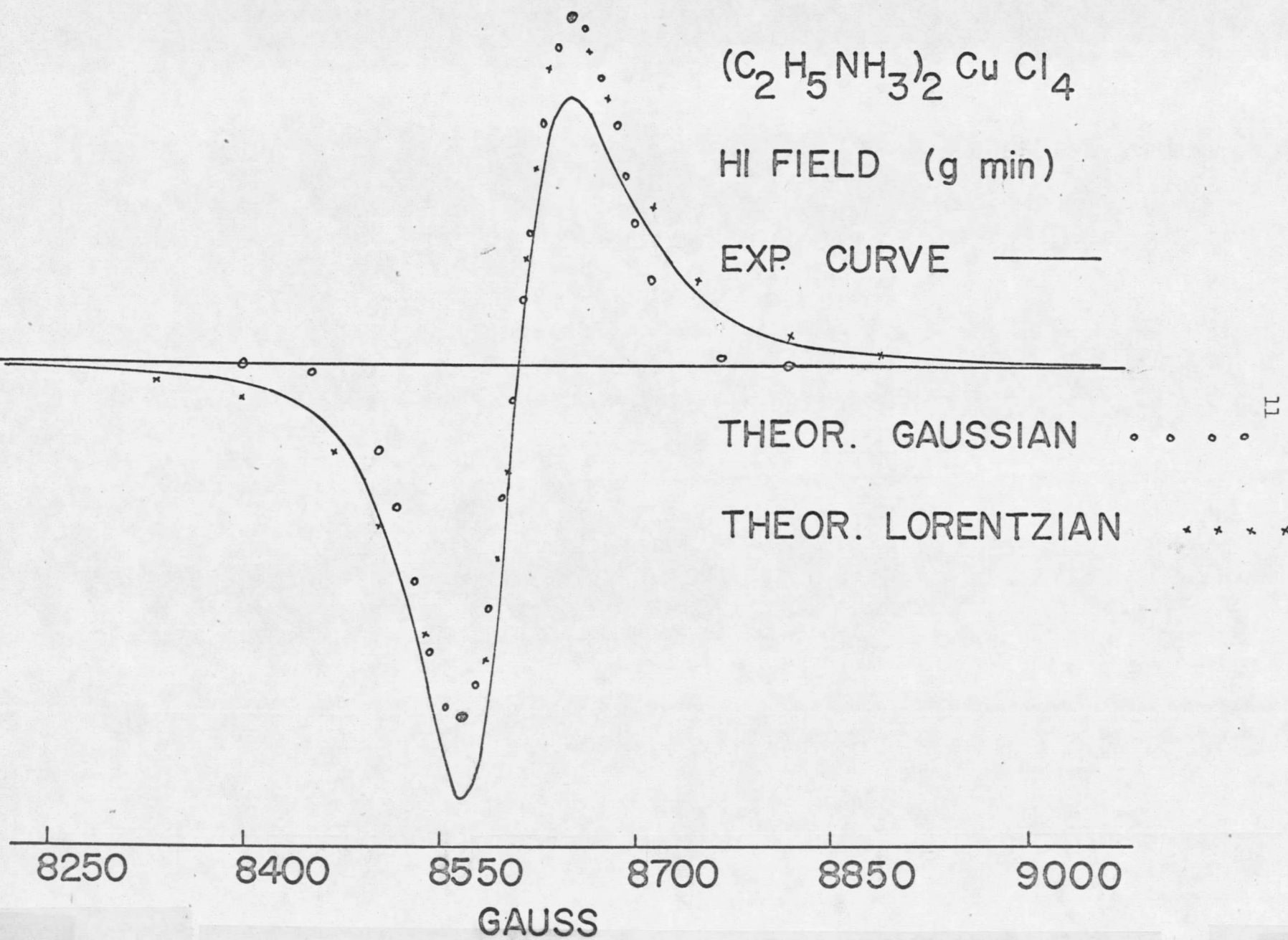
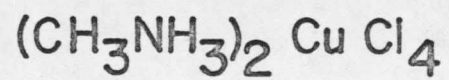


Figure 5. EATCC



LOW FIELD (g max.)

EXP. CURVE ———

THEOR. GAUSSIAN ○ ○ ○ ○ 12

THEOR. LORENTZIAN × × × ×

7950 8150 8350 8550 8750
GAUSS

Figure 6. MATCC

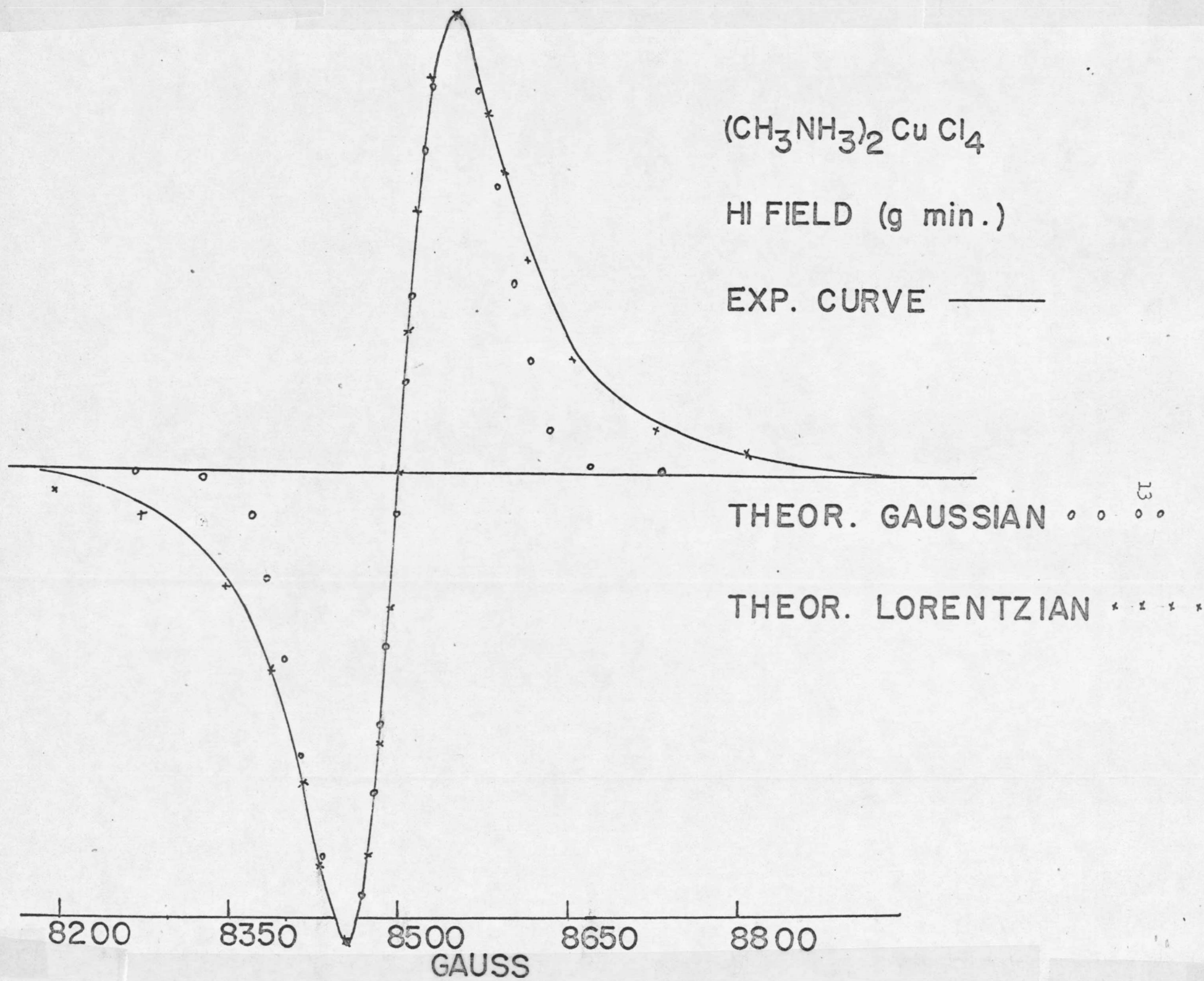
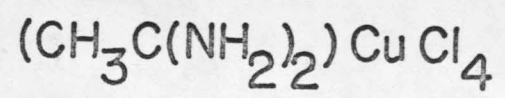


Figure 7. MATCC



HI FIELD

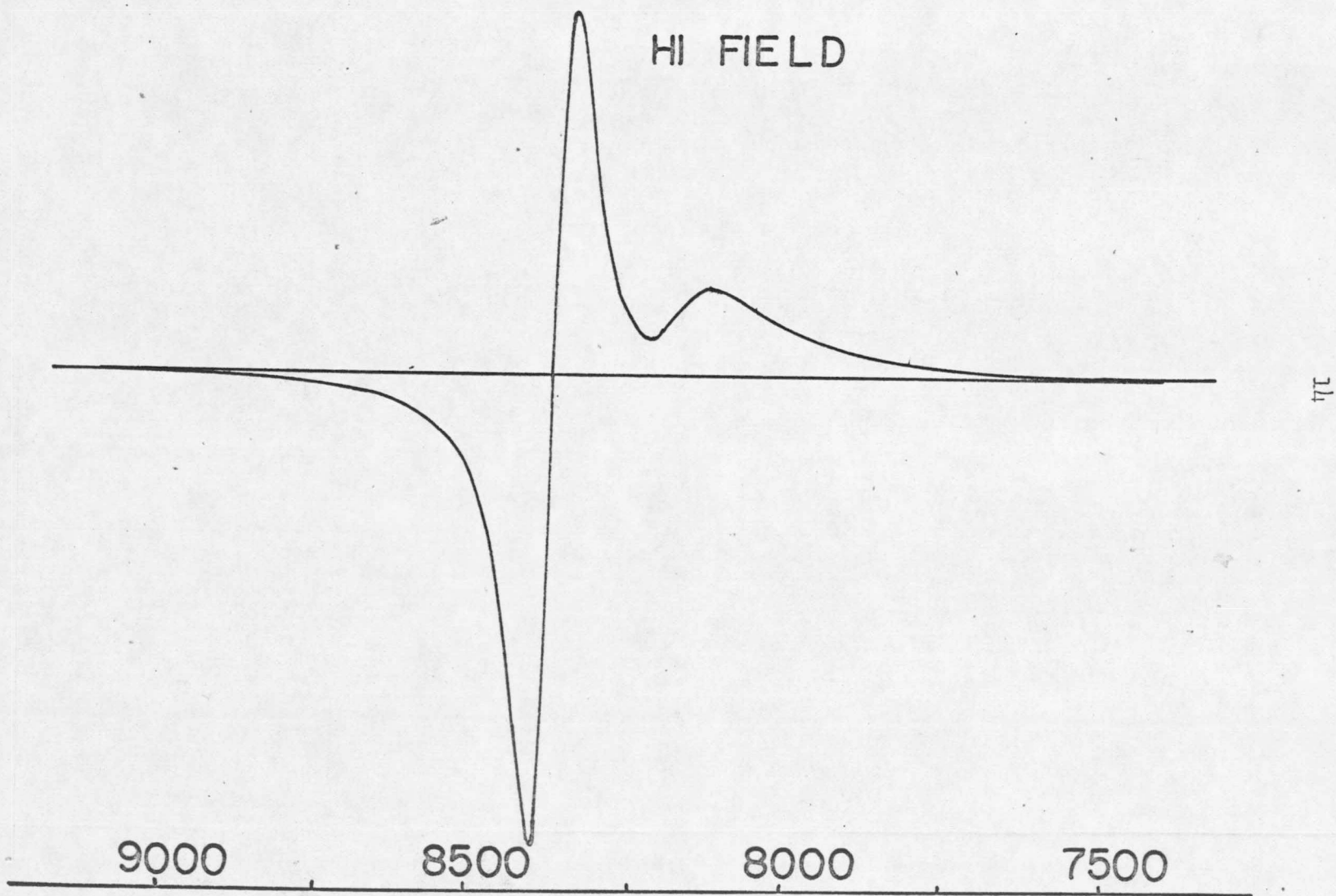


Figure 8. ACTCC

The g values in MATCC and EATCC are anisotropic and are characterized by the g tensor which has the principal values g_{xx} , g_{yy} , and g_{zz} where the z axis is the long bond axis of the distorted octahedron. Often this tensor has axial symmetry, in which case $g_{xx} = g_{yy} = g_{\perp}$ and $g_{zz} = g_{\parallel}$. This was the assumption made by Willett et al.¹¹ Since the electron g value is related to the Cu-Cl bond length and since x is not equal to y in EATCC and MATCC, it is to be expected that g_{xx} would not equal g_{yy} . Since $g_{xx} = g_{\min} = g_{\perp}$ and $\frac{1}{2}(g_{yy} + g_{zz}) = g_{\max}$, where $g_{zz} = g_{\parallel}$, g_{yy} must be determined in order to determine g_{\parallel} . Since x is related to g_{xx} , etc. it was thought that g_{\max} must be related to $\frac{y+z}{2}$. This was confirmed by calculations with $\frac{x+z}{2}$ as related to $\frac{g_{xx} + g_{zz}}{2}$. Using a graphical solution, the data tabulated in Table II was obtained.

TABLE II

Crystal	$g_{xx} = g_{\perp}$	g_{yy}	$g_{zz} = g_{\parallel}$
EATCC	2.053	2.067	2.261
MATCC	2.054	2.068	2.270

The data in

The data in Table II leads to the conclusion that the ratio of the square root of the bond lengths is approximately equal to the ratio of the g values.

The Cu-Cl-Cu paramagnetic electron super exchange frequency has been

calculated using the following calculation from Pake:³

$\omega_d^2 = \kappa \Omega^2 = (3/4)S(S+1)\hbar^{-2} \sum_j g_j^4 \beta^4 r_{jk}^{-6} (3\cos^2 \Theta_{jk} - 1)^2$, where S is the spin quantum number which is equal to $\frac{1}{2}$ for Cu^{++} , $g = 2.164$ for EATCC and 2.169 for MATCC, r is the distance between the Cu^{++} ions and is 5.125×10^{-8} cm, Θ_{jk} is the angle from the z axis of a typical interior ion site k to any other interacting atom j, the sum being carried out over the nearest neighbor sites only, and ω_d is the dipolar exchange frequency.

$\Delta\omega_{\frac{1}{2}} = \frac{\pi}{2} \frac{\omega_d^2}{\omega_e}$, where $\Delta\omega_{\frac{1}{2}}$ is the angular frequency half width and ω_e is the Cu-Cl-Cu electron super exchange frequency. $\Delta\omega_{\frac{1}{2}} = \frac{g\beta}{\hbar} \Delta H_{\frac{1}{2}}$, where $\Delta H_{\frac{1}{2}}$ is the line width in gauss at half maximum amplitude. Finally, $\Delta H_{\frac{1}{2}} = \sqrt{3} \Delta H_{pp}$, where ΔH_{pp} is the peak to peak line width given in Table I.³

The calculated values of ω_e are, for EATCC and MATCC respectively, 20.39 GHz and 17.48 GHz.

Chapter IV: The Spectrometer

The Spectrometer

The k-band spectrometer constructed for this experiment is a high frequency modulation spectrometer utilizing a reflection cavity. A block diagram of the spectrometer is shown in Figure Nine. Most of the spectrometer was assembled with commercially manufactured equipment. The pieces built "in house" were the cavity, the 125 KHz modulation oscillator-amplifier,¹⁴ the modulation coils, the nuclear magnetic resonance (NMR) probe,¹⁵ and a low temperature cavity mount.¹⁶

The klystron is an OKI model 24V10A which can be made to oscillate over the range 22.0 to 26.0 GHz. The klystron is mounted in a TRG model 946A oil bath mount to maintain the klystron at a stable temperature level and thus improve the frequency stability. The klystron is powered by a Narada Microline model 621A power supply with a Kepco model ABC voltage regulated klystron filament supply. The klystron frequency drift is controlled by a Teltronics model KSLP klystron stabilizer which applies a 70 KHz signal to the reflector of the klystron, phase detects the output, and provides a d.c. correction voltage to the reflector. The klystron is effectively isolated with a minimum isolation of 24 db from any reflected microwaves by the PRD model 1209F1 isolator. The Waveline, Inc. model 812 calibrated attenuator (0 to 40 db) serves to reduce the effective power output of the klystron. It is necessary to have an attenuator since the klystron is a fixed power output device.

A Waveline, Inc. model 869-20 db cross guide coupler splits the signal from the klystron into two signals: the larger of which goes to the Ferrotec, Inc. model T380 3 port ferrite circulator and the smaller of which

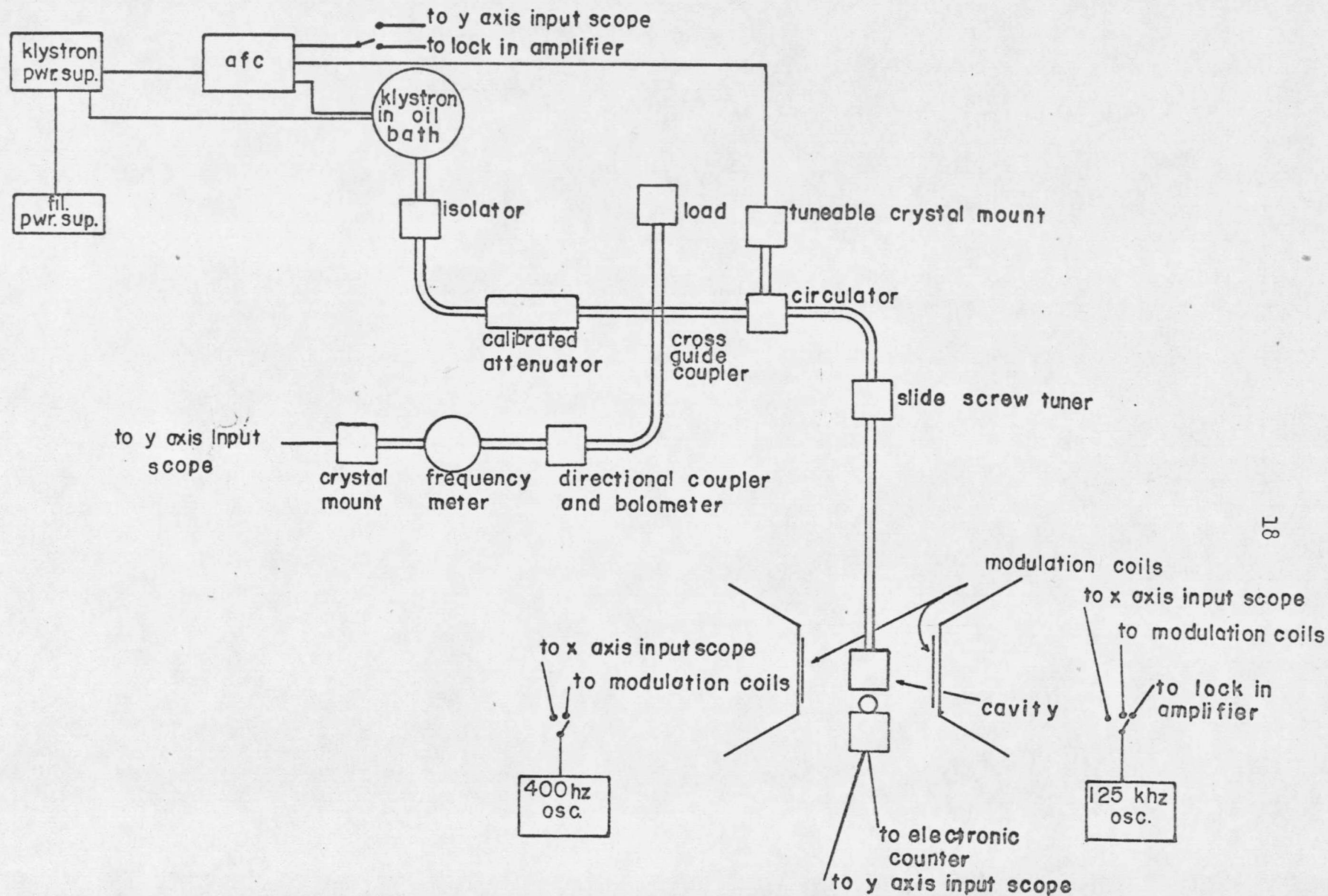


Figure 9.
K BAND REFLECTION SPECTROMETER

goes to the Narda Microwave Corporation model 1068-3 db directional coupler. The signal reflected from the circulator returns to the cross guide coupler and splits, part of which returns to the attenuator and the other part of which terminates in a Waveline, Inc. model 854 matched load.

The 3 db directional coupler splits the signal from the 2 db cross guide coupler into two components, one of which goes to a Hewlett-Packard model K532A precision direct reading frequency meter, and the other of which goes to the PRD model 621A bolometer. The signal from the precision direct reading frequency meter can then be detected in a Waveline, Inc. model 816 crystal mount with a 1N26 diode. The signal from the circulator goes to the Waveline, Inc. model 883 slide screw tuner and from there to the cavity. The slide screw tuner can be thought of as a variable impedance which can be adjusted to match the impedance of the detector arm to the impedance of the cavity arm. Its effect is to tune out any standing waves in the waveguide, i.e., to reduce the power transfer along the waveguide. The reflected radiation passes through the slide screw tuner to the circulator and from there to the PRD model 621AF tuneable crystal mount, which is also equipped with a 1N26 detection diode.

The associated equipment for the spectrometer will be briefly described. A Tektronix, Inc. type 545A oscilloscope with either a type B or type E plug-in unit was used to monitor the signals from both the tuneable and fixed crystal mounts, the 125 KHz modulation and the signal from the NMR probe. The 125 KHz oscillator-amplifier was used to add a modulated component to the static magnetic field. Figures Ten and Eleven show the circuit diagrams of the oscillator-amplifier and the amplifier. The

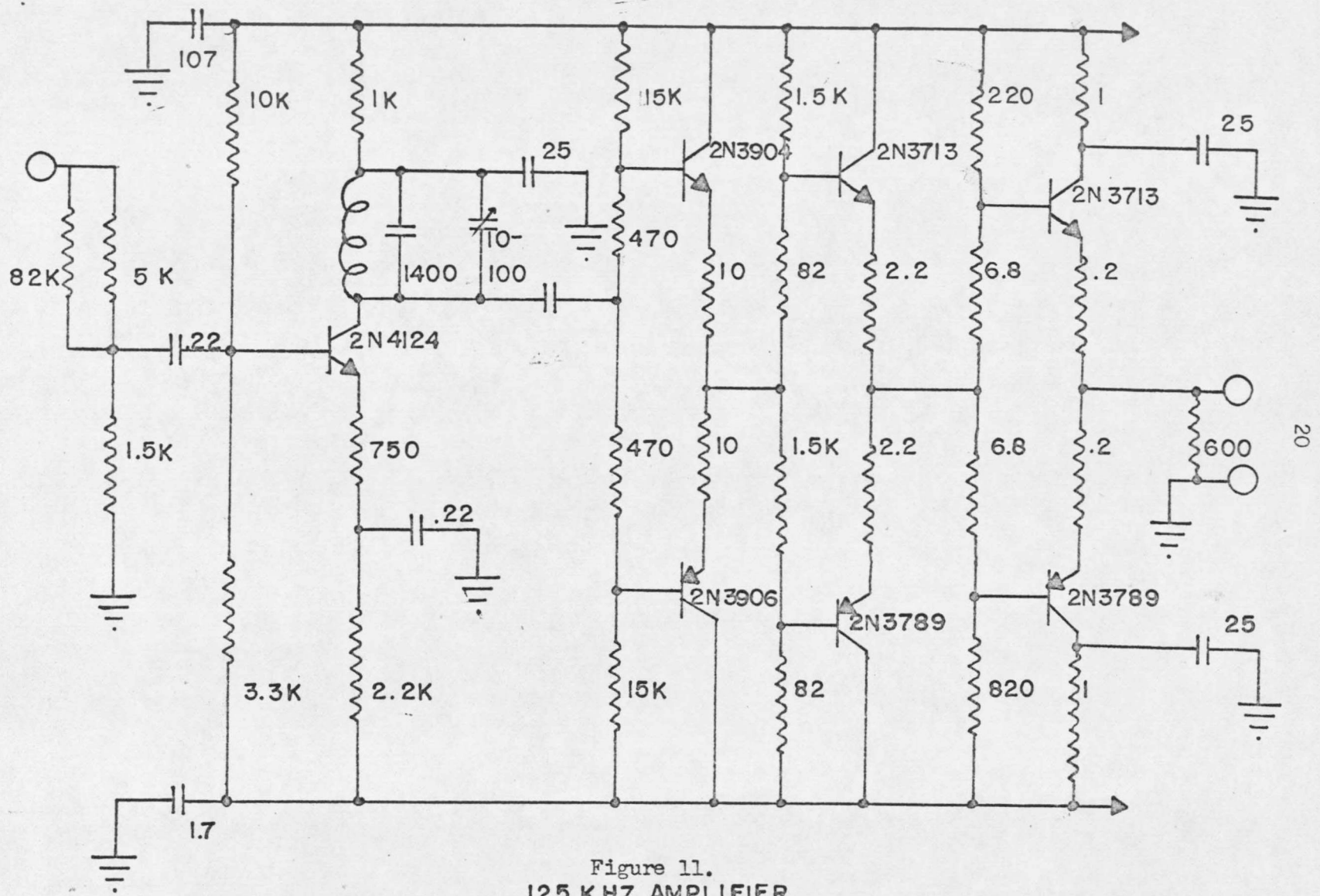


Figure 11.
125 KHZ AMPLIFIER
CHANNEL 2

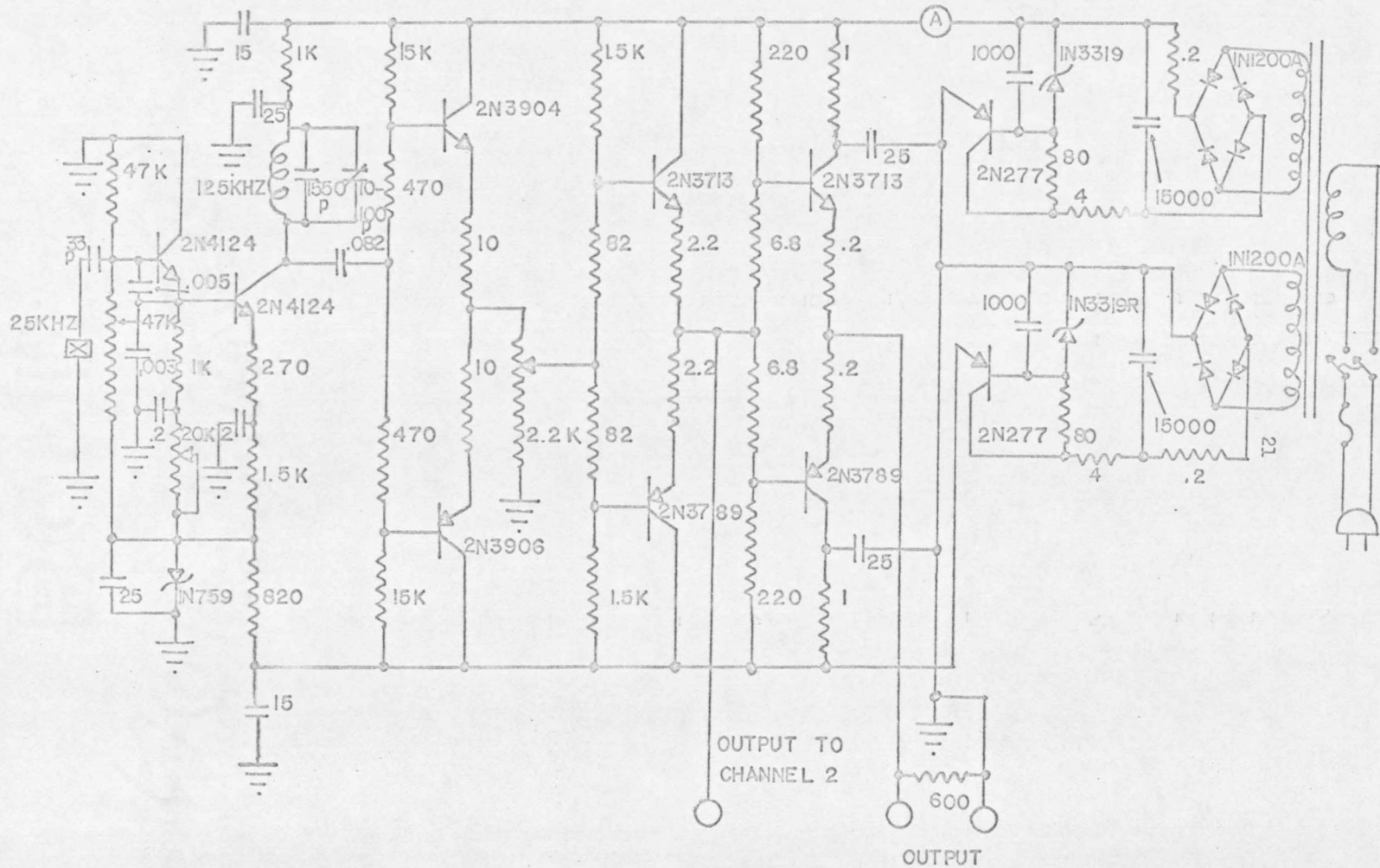


Figure 10.
125KHZ OSCILLATOR AMPLIFIER

The nuclear magnetic resonance (NMR) probe was used to determine an accurate value of the magnetic field at resonance and a Hewlett-Packard model 5246L electronic counter was utilized to determine the oscillation frequency of the NMR oscillator. The Hewlett-Packard model 200 AB audio oscillator was used to modulate the magnetic field at 400 Hz. A Princeton Applied Research Corporation model 121 lock-in amplifier/phase detector (PAR) was used to detect the absorption of energy from the microwave field in the cavity at resonance. Both a Varian model G 14A-1 graphic recorder and a Hewlett-Packard model 7000 AR x-y recorder were used to record the data. A Fieldial model VFR2503 Varian field regulated magnet power supply was used to control a Varian model V-3400 electromagnet.

A variable temperature cavity mount, shown in Figure Twelve, was used at room temperature. This mount will also be used to support the cavity in low temperature dewars for possible variable temperature work. The fixed frequency cavity was designed to resonate at 24.7 GHz.

The TE_{011} resonant mode was chosen for central positioning of the crystal in the region of maximum magnetic field and minimum interference with the electric field. As can be seen in Figure Thirteen, the perturbing magnetic field is always perpendicular to the level splitting (Zeeman) magnetic field, thus allowing the rotation of the field about the vertical axis with no loss in intensity.

The cavity used was constructed in three steps: 1. A .600 inch inner diameter hole was cut in brass stock, the outer surface of which was cut to .654 inches. 2. A .650 inch inner diameter hole was cut in low temperature plastic. 3. With the plastic piece centered in the lathe, the brass was

